Applied Catalysis B: Environmental 147 (2014) 789–795

Contents lists available at ScienceDirect

Applied Catalysis B: Environmental

journal homepage: www.elsevier.com/locate/apcatb

Hydrogen peroxide assisted rapid synthesis of TiO_2 hollow microspheres with enhanced photocatalytic activity

Yang Zheng, Jinghua Cai, Kangle Lv*, Jie Sun, Hengpeng Ye, Mei Li

Key Laboratory of Catalysis and Materials Science of the State Ethnic Affairs Commission & Ministry of Education, South-Central University for Nationalities, Wuhan 430074, PR China

ARTICLE INFO

Article history:
Received 15 July 2013
Received in revised form 2 October 2013
Accepted 7 October 2013
Available online 16 October 2013

Keywords:
TiO_2 hollow microspheres
Photocatalysis
Hydrogen peroxide
Fluoride-induced self-transformation (FIST)

ABSTRACT

Anatase TiO_2 hollow microspheres (TiO_2-HMSs) have attracted great attention owing to their versatile applications including photocatalysis, sensing, lithium-ion batteries, drug-delivery carrier and solar energy conversion. However, the synthetic procedures for TiO_2-HMSs are complex and/or time-consuming. In this paper, rapid synthesis of TiO_2-HMSs in the presence of H_2O_2 (0–4.4 mol) was systematically studied by hydrothermal treatment of the mixed solution of $(NH_4)_2TiF_6$ (6 mmol) and $(NH_4)_2CO$ (40 mmol). It was found that the diameters of the obtained spherical TiO_2 aggregates decreases with increase in the amount of H_2O_2, and H_2O_2 not only promotes the crystallization of primary anatase TiO_2 nanocrystals, but also induces the hollowing process of TiO_2 microspheres. The prepared TiO_2-HMSs shows high photocatalytic activity in degradation of Brilliant Red X-3B, an anionic dye, under UV irradiation due to H_2O_2-mediated enhanced crystallization and improved adsorption. A proposed formation mechanism was put forward for the rapid formation of TiO_2-HMSs based on H_2O_2-assisted nucleation, and followed by fluoride-induced self-transformation (FIST).

1. Introduction

As one of oxide semiconductor photocatalysts, TiO_2 has proven the most suitable for widespread environmental applications due to its biological and chemical inertness, strong oxidizing power, cost-effectiveness, and long-term stability against photocorrosion and chemical corrosion [1–5]. However, the performance of TiO_2 needs to be improved from the viewpoint of practical applications due to low quantum efficiency [3,6–9].

Recently, TiO_2 hollow structures have attracted great attention due to their high surface-to-volume ratio, lower density, better permeation, and high photocatalytic activity [10–18]. The well-established strategies for fabrication of TiO_2 hollow microspheres (TiO_2-HMSs) including conventional hard-templating [13,19–23] and soft-templating methods [24–27] have been reported. Because of the complexity of the aforementioned templating strategies, the template-free methods, such as fluoride induced self-transformation (FIST) based on Ostwald ripening, have been recently developed to fabricate TiO_2-HMSs [7,12,28–34]. The fabrication of TiO_2-HMSs by FIST has been characterized by the following 4 steps (example using $(NH_4)_2TiF_6$ as titanium and fluoride source) [35,36]: (1) hydrolysis of titanium salt and nucleation of metastable TiO_2 nanoclusters (Eq. (1)), (2) spontaneous organization of the incipient nanoclusters into amorphous spherical aggregates in solid form, (3) heterogeneous nucleation of a crystalline thin shell around the amorphous microparticles, and (4) fluoride induced preferential dissolution of the amorphous particle interior and concurrent deposition of a porous crystalline external shell to produce intact hollow microspheres without significant modification in the bulk particle morphology (Eqs. (2) and (3)).

$$TiF_6^{2-} + 2H_2O \rightarrow TiO_2\,(\text{amorphous}) + 4H^+ + 6F^- \quad (1)$$

$$4H^+ + TiO_2\,(\text{amorphous}) + 6F^- \rightarrow TiF_6^{2-} + 2H_2O\,(\text{dissolution}) \quad (2)$$

$$TiF_6^{2-} + 2H_2O \rightarrow 4H^+ + TiO_2\,(\text{anatase}) + 6F^-\,(\text{recrystallization}) \quad (3)$$

Yang and Zeng [37] first reported the controlled synthesis of TiO_2-HMSs via hydrolysis of acidic TiF_4 solution at 200 °C for 24 h. Subsequently, a modified synthetic approach involving the hydrothermal treatment of acidic $Ti(SO_4)_2$ solution in the presence of NH_4F at 180 °C for 12 h was developed for the fabrication of anatase TiO_2-HMSs [30]. However, these methods for fabrication of TiO_2-HMSs are time-consuming and energy-wasting. Rapid

* Corresponding author. Tel.: +86 27 67842752; fax: +86 27 67842752.
E-mail addresses: lvkangle@mail.scuec.edu.cn, lvkangle888@163.com (K. Lv).

0926-3373/$ – see front matter © 2013 Elsevier B.V. All rights reserved.
http://dx.doi.org/10.1016/j.apcatb.2013.10.011

synthesis of TiO_2-HMSs at low temperature is urgently needed but remains a great challenge [38].

Our group have recently reported the synthesis of high photo-reactive rugby-like TiO_2 hollow nanoparticles (TiO_2-HNPs) by hydrothermal treatment of $Ti(OC_4H_9)_4$–NH_4HF_2–H_2O_2 mixed solution at 150 °C for 10 h [39], and hierarchical TiO_2-HMSs assembly by TiO_2-HNPs by a simple hydrothermal route in a $Ti(SO_4)_2$–NH_4F–H_2O_2 mixed solution at 180 °C for 3 h [40]. Both of these work suggest that H_2O_2 can influence the formation of anatase TiO_2 hollow interiors. In this paper, we reported the rapid fabrication of chain-like anatase TiO_2-HMSs assemblies in the presence of H_2O_2 by hydrothermal treatment of the mixed solution of $(NH_4)_2TiF_6$ and urea ($(NH_4)_2CO$) at low temperature of 150 °C for only 3 h. The synthesized TiO_2-HMSs show overwhelming better performance than TiO_2 solid microspheres prepared under other identical condition in the absence of H_2O_2. A possible mechanism for the rapid fabrication of TiO_2-HMSs was proposed based on H_2O_2-assisted nucleation and followed by FIST hollowing process.

2. Experimental

2.1. Preparation

Chain-like TiO_2-HMSs were prepared by hydrothermal treatment of $(NH_4)_2TiF_6$ aqueous solution in the presence of urea and H_2O_2. In a typical synthesis, 2.42 g urea (40 mmol) was added into 50 ml solution dissolving 6 mmol $(NH_4)_2TiF_6$ under vigorous stirring. Then, 30 ml H_2O_2 (40 wt%, 4.4 mol) was dropwise added into the mixed solution, forming a characteristic deep orange solution. The resulted solution was transferred to a 100 ml Teflon-lined autoclave, which was sealed and kept at 150 °C for 3 h. After cooling to room temperature, the obtained precipitate was filtrated. To eliminate the surface adsorbed fluoride ions, the precipitate was washed by 0.1 M NaOH, followed by distilled water until the pH value of the filtrate is about 7 before drying at room temperature [9]. For comparison, a serial samples were also prepared (Table 1). The prepared TiO_2 sample is labeled as S_{x-y}, where suffix "x" and "y" represent the volumes of H_2O_2 (x ml) and the reaction time (y h), respectively. For example, the sample $S_{30\text{-}3}$ represents the sample prepared in the presence of 30 ml H_2O_2 at 150 °C for 3 h. Note that the total volume of the mixed solution in hydrothermal reaction is kept the same (80 ml) for all TiO_2 samples.

2.2. Characterization

The X-ray diffraction (XRD) patterns obtained on a D8-advance X-ray diffractometer (German Bruker). The accelerated voltage and applied current were 15 kV and 20 mA, respectively. The average crystalline size of the catalyst was determined according to the Scherrer equation using full width at half maximum data after correcting for the instrumental broadening. The morphology of TiO_2 powders was observed on a transmission electron microscope (TEM) (Tecnai G20, USA) using an acceleration voltage of 200 kV and a field emission scanning electron microscope (FESEM) (S-4800, Hitachi, Japan) with an acceleration voltage of 10 kV, respectively. Nitrogen adsorption–desorption isotherms were obtained on an ASAP 2020 (Micromeritic Instruments, USA) nitrogen adsorption apparatus. All the samples were degassed at 120 °C prior to Brunauer–Emmett–Teller (BET) measurements. The BET specific surface area (S_{BET}) was determined by a multipoint BET method using the adsorption data in the relative pressure P/P_0 range of 0.05–0.30. The desorption isotherm was used to determine the pore size distribution by using the Barret–Joyner–Halenda (BJH) method. The nitrogen adsorption volume at $P/P_0 = 0.994$ was used to determine the pore volume (PV) and average pore size (APS).

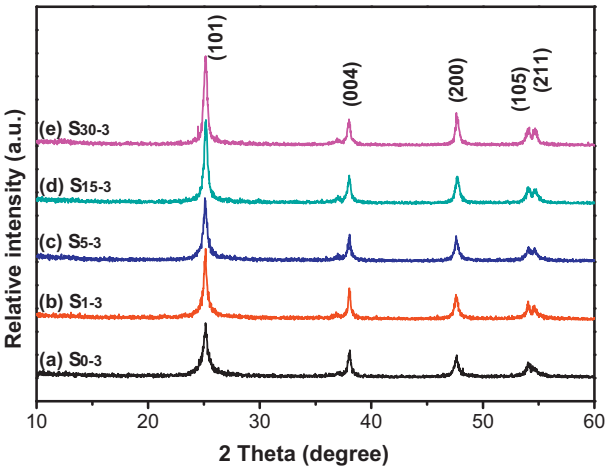

Fig. 1. XRD patterns of TiO_2 samples for $S_{0\text{-}3}$(a), $S_{1\text{-}3}$(b), $S_{5\text{-}3}$(c), $S_{15\text{-}3}$(d), $S_{30\text{-}3}$(e), respectively.

2.3. Evaluation of the photocatalytic activity

A 3W LED lamp (UVEC-4 II, Shenzhen lamplic, China) emitted mainly at 365 nm is used as light source, which is placed outside a Pyrex-glass reactor at a fixed distance (ca. 5 cm). Brilliant Red X-3B (X3B) [3,41,42], an anionic azo dye is used as a probe molecule. During the photocatalytic reaction, the reactor was mechanically stirred at a constant rate. The concentration of TiO_2 was 1.0 g/L, and the initial concentration of X3B was 1.0×10^{-4} mol/L. Before irradiation, the suspensions were sonicated first for 5 min, and then were shaken overnight in the dark to establish the adsorption–desorption equilibrium. At given intervals of irradiation, small aliquots were withdrawn by a syringe, and filtered through a membrane (pore size 0.22 μm). The concentration of X3B remaining in the filtrate was then analyzed by an Agilent 8451 spectrometer at 510 nm.

3. Results and discussion

3.1. Phase structure and morphology

The phase structure, crystallite size (crystallinity) of TiO_2 are of great importance for its photocatalytic activity [3]. XRD was used to investigate the effect of H_2O_2 and reaction time on the phase structure and crystallinity of TiO_2 samples. As shown in Fig. 1, all X-ray diffraction (XRD) peaks of the aspreparedTiO$_2$ samples match the anatase phase of TiO_2. The broadening of the diffraction peak at $2\theta = 25.3°$ corresponding to (1 0 1) plane diffraction for $S_{0\text{-}3}$ sample is caused by the small crystallite size and weak crystallization of the sample. It can be seen that the peak intensity of anatase increases with increase in the amount of H_2O_2 from 0 to 30 ml, indicating an enhancement of crystallization [39,40]. Meanwhile, the width of the (1 0 1) plane diffraction peaks became narrower, showing an increase in anatase crystallite size (Table 1). The study of Du et al. [43] have proposed that the hydrolyzed TiO_2 clusters can connect with each other through ≡Ti···O—O···Ti≡ bridge in the presence of H_2O_2. Such bounding should facilitate the growth and crystallization of TiO_2 particles.

Fig. 2 shows the effect of H_2O_2 on the formation of TiO_2-HMSs. In the absence of H_2O_2, only solid spherical TiO_2 aggregates were obtained even extension the reaction time from 3 to 48 h (Fig. 2a and b), reflecting the slow Ostwald ripening (or FIST) process. It can

Table 1
Starting materials and XRD characterization results of the photocatalysts.

Catalyst	Starting materials				X3B adsorbed (μmol g^{-1})[a]	Crystalline size (nm)	Relative crystallinity[b]
	$(NH_4)_2TiF_6$(g)	$(NH_4)_2CO$ (g)	H_2O_2(ml)	H_2O (ml)			
$S_{0\text{-}3}$	1.19	2.42	0	80	0.10	13.1	1
$S_{1\text{-}3}$	1.19	2.42	1	79	0.48	17.0	1.07
$S_{5\text{-}3}$	1.19	2.42	5	75	0.57	17.2	1.11
$S_{15\text{-}3}$	1.19	2.42	15	65	1.91	20.4	1.49
$S_{30\text{-}3}$	1.19	2.42	30	50	2.18	21.8	1.53

[a] Amount of X3B dye adsorbed on the surface of TiO_2 before photocatalytic degradation.
[b] Relative anatase crystallinity: the relative intensity of the diffraction peak from the anatase (1 0 1) plane (sample $S_{0\text{-}3}$ is used as reference).

also be seen from Fig. 2a that the diameters of the spherical TiO_2 aggregates are in the range of 1–5 μm with poor monodispersity. However, the morphology of TiO_2 sample was found to evolve from solid to core/shell structured and hollow spherical aggregates with increase in the amount of H_2O_2 under other identical conditions. From the TEM images, it can also be seen that the diameters of the monodisperse TiO_2 microspheres steady decease from about 1.5 to 0.6 μm with increase in the amount of H_2O_2 from 1 ml to 30 ml.

Enhanced crystallization and accelerating the evacuation of spherical TiO_2 aggregates by H_2O_2 were also observed for samples prepared at 150 °C for 10 h (Fig. S1 and Fig. 3). No TiO_2-HMSs can be obtained in the absence of H_2O_2 even extension the reaction time to 48 h (Fig. 2b). However, TiO_2-HMSs were formed at 150 °C for only 3 h when 30 ml H_2O_2 was added (Fig. 2f), reflecting the importance of H_2O_2 on the formation of hollow interiors. Further study shows that the yield of TiO_2 sample almost keeps unchanged whatever the presence or absence of H_2O_2. These results indicate that H_2O_2 can enhance the nucleation of TiO_2 precursors, which results in the decrement in diameters of TiO_2 microspheres with increase in the amount of H_2O_2 (Figs. 2 and 3).

Fig. 4 shows the effect of hydrothermal reaction time on the crystallization of TiO_2 sample prepared in the presence of 15 ml H_2O_2. It can be seen that the crystallization of anatase TiO_2 enhances with increasing the reaction time from 3 to 48 h. Similar results were also found for samples prepared in the presence of 1 ml H_2O_2 (Fig. S2). This is due to the self-transformation of amorphous into anatase TiO_2-HMSs (Eqs. (1)–(3)). Transformation occurs with retention of the bulk morphology by localized Ostwald ripening (or FIST), where preferential dissolution of the particle interior is coupled to the deposition of a porous external shell of loosely packed nanocrystals [7,35]. This shape evolution can also be clearly seen from the sample prepared in the presence of 1 ml H_2O_2 with extension the reaction time from 3 h to 48 h (compared Fig. 2c with Figs. 3a and 5a, b).

Fig. 6 shows the SEM images of TiO_2 samples, where the shape evolution from solid microspheres to hollow microspheres can be clearly observed. From Fig. 6d and f, it can be seen that the average crystallite sizes on the outer surface are much larger than these in the inner cores of the core–shell structured TiO_2 microspheres, confirming that the Ostwald ripening is responsible for the formation of TiO_2-HMSs. Inside-out Ostwald ripening is a spontaneous process, which was first described by Wilhelm Ostwald in 1896,

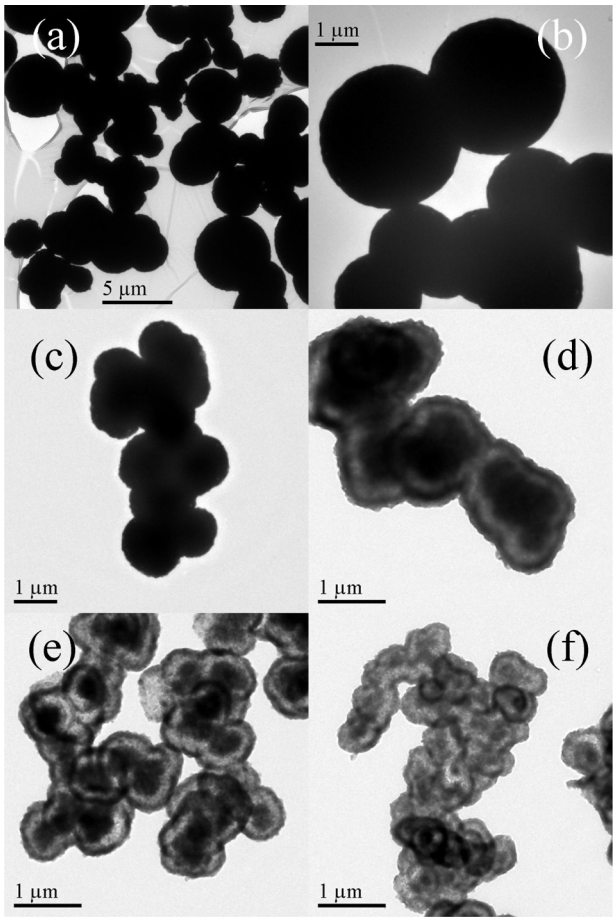

Fig. 2. TEM images of TiO_2 samples after hydrothermal treatment at 150 °C for 3 h in the absence ($S_{0\text{-}3}$, a) and presence of 1 ml ($S_{1\text{-}3}$, c), 5 ml ($S_{5\text{-}3}$, d), 15 ml ($S_{15\text{-}3}$, e) and 30 ml ($S_{30\text{-}3}$, f) of H_2O_2, respectively. Image b is the sample prepared at 150 °C for 48 h in the absence of H_2O_2 ($S_{0\text{-}48}$) for comparison.

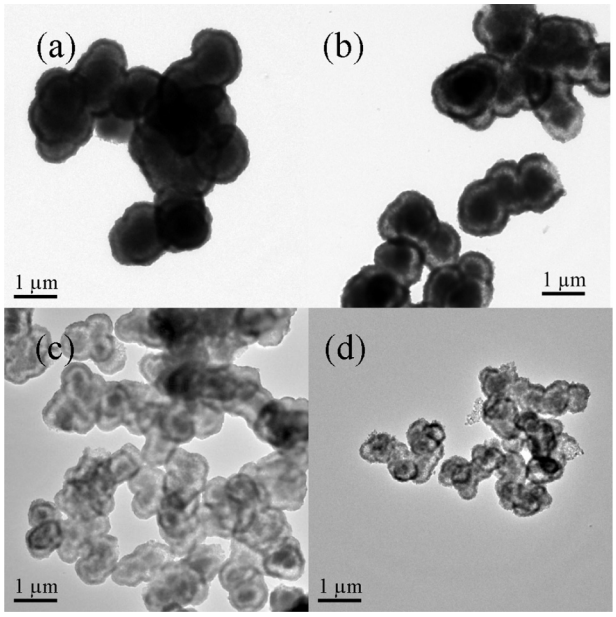

Fig. 3. TEM images of TiO_2 samples after hydrothermal treatment at 150 °C for 10 h in the presence of 1 ml ($S_{1\text{-}10}$, a), 5 ml ($S_{5\text{-}10}$, b), 15 ml ($S_{15\text{-}10}$, c) and 30 ml ($S_{30\text{-}10}$, d) of H_2O_2, respectively.

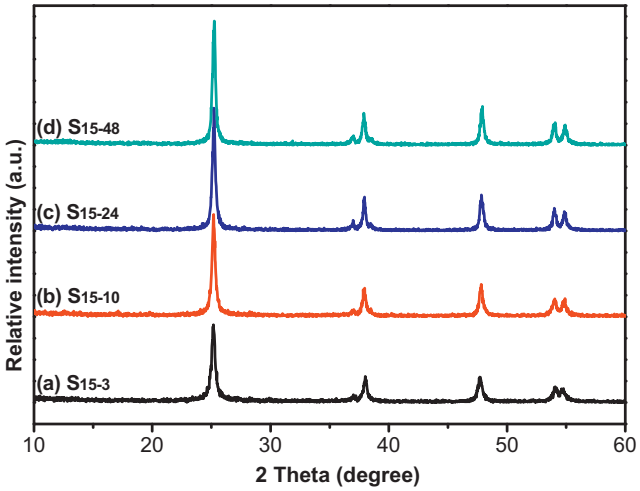

Fig. 4. XRD patterns of the TiO_2 samples for $S_{15\text{-}3}$ (a), $S_{15\text{-}10}$ (b), $S_{15\text{-}24}$ (c) and $S_{15\text{-}48}$ (d), respectively.

refering to the growth of large precipitates at the expense of smaller precipitates caused by energetic factors [10]. Since the average crystallite sizes in inner cores are smaller than these on the outer surface, nanocrystals in inner cores have a tendency to dissolve, which steadily recrystallize on the outer surface, till the formation of hollow interiors (mass transfer from core to shell).

Fig. 7 depicts the effect of H_2O_2 on the hollowing process of TiO_2 microspheres. It can be seen that H_2O_2 not only enhances the formation of hollow interiors, but also influence the diameters of the resulted TiO_2-HMSs. In the absence of H_2O_2, only TiO_2 solid microspheres with poor monodispersity in diameters of about 1–5 μm can be obtained even extension the reaction time to 48 h (Fig. 2b). However, monodisperse TiO_2-HMSs in diameters of 0.6 μm was fabricated after reaction for 3 h in the presence of 30 ml H_2O_2 (Fig. 2f). H_2O_2 can also affect the wall thickness of the obtained TiO_2-HMSs. Larger amount of H_2O_2 results in the formation of TiO_2-HMSs with thinner wall thickness (Fig. 6).

3.2. Nitrogen adsorption–desorption isotherms

To get more information about the microstructures of the obtained TiO_2-HMSs, nitrogen adsorption–desorption isotherms were measured. The isotherms of the TiO_2 samples shown in Fig. 8 are of type IV (BDDT classification). The corresponding pore size distribution curves show that TiO_2-HMSs of S1-3 only contain small mesopores (about 4 nm), while $S_{1\text{-}10}$ and $S_{15\text{-}10}$ have both small and larger mesopores (inset of Fig. 8). This is due to the formation of hollow interiors of $S_{1\text{-}10}$ and $S_{15\text{-}10}$ samples. According to previous reports, a bimodal mesopore size distribution results from two different aggregates in the powders. The hysteresis loop in the lower relative pressure range ($P/P_0 < 0.4$) is related to finer intra-aggregated pores formed between intra-agglomerated primary particles, and that in the higher relative pressure range ($0.4 < P/P_0 < 1$) is associated with larger interaggregated pores produced by interaggregated secondary particles [26]. H_2O_2 and reaction time exerted significant influence on the pore structure and BET surface areas of the obtained products. The isotherms corresponding to $S_{1\text{-}10}$ TiO_2-HMSs show higher absorption at high relative pressures (P/P_0 approaching 1) than $S_{1\text{-}3}$ TiO_2 solid microspheres, indicating the formation of macropores and/or an increasing pore volume with extension the reaction time. The PV and APS of the photocatalyst prepared in the presence of 1 ml H_2O_2 increased from 0.038 $cm^3\ g^{-1}$ and 3.8 nm ($S_{1\text{-}3}$) to 0.060 $cm^3\ g^{-1}$ and 7.1 nm ($S_{1\text{-}10}$), respectively, when the reaction time was increased from 3 h to 10 h (Table 2). The increment of PV and APS is related to the H_2O_2-mediated hollowing of the interior space of TiO_2 microspheres (as shown in Figs. 2c and 3a). The concentration of H_2O_2 can also affect the pore structure of TiO_2-HMSs. The hysteresis loops in the higher relative pressure range ($0.4 < P/P_0 < 1$) of the samples prepared at 150 °C for 10 h shifted upward with increase in the amount of H_2O_2 from 1 ml to 15 ml, suggesting that the PV of interaggregated pores increased (Table 2) [26]. From Table 2 it can be found that the BET specific areas of the photocatalysts decrease with increase in the amount of H_2O_2 or extension the reaction time. This is due to the enhanced crystallization of TiO_2 samples (Figs. 1, 4 and 6) [39].

Table 2
Nitrogen adsorption–desorption characterization results of the photocatalysts.

Catalyst	Characterization results		
	S_{BET} ($m^2\ g^{-1}$)	PV ($cm^3\ g^{-1}$)	APS (nm)
$S_{1\text{-}3}$	39.5	0.038	3.8
$S_{1\text{-}10}$	36.1	0.060	7.1
$S_{1\text{-}24}$	30.8	0.063	8.2
$S_{15\text{-}3}$	54.4	0.067	4.9
$S_{15\text{-}10}$	37.2	0.090	9.7
$S_{15\text{-}24}$	38.3	0.082	8.6

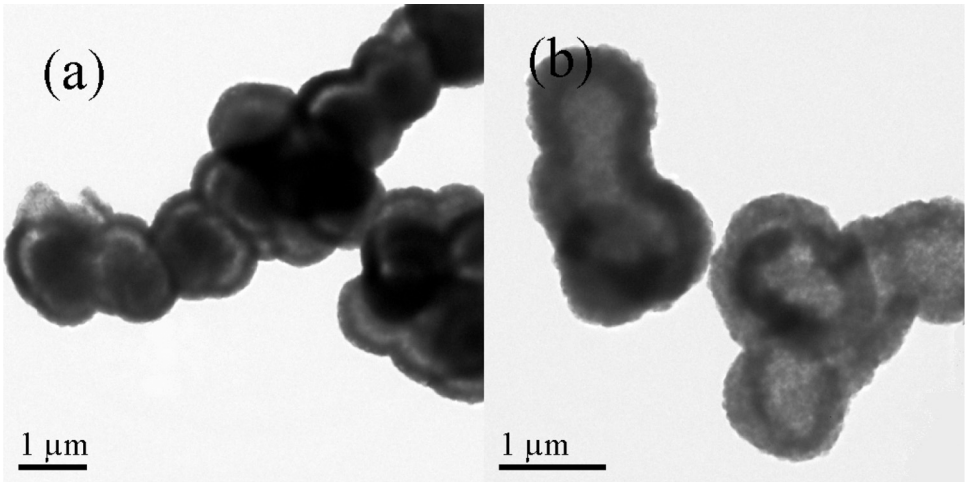

Fig. 5. TEM images of TiO_2 samples prepared in the presence of 1 ml of H_2O_2 after hydrothermal treatment at 150 °C for 24 h (a) and 48 h (b), respectively.

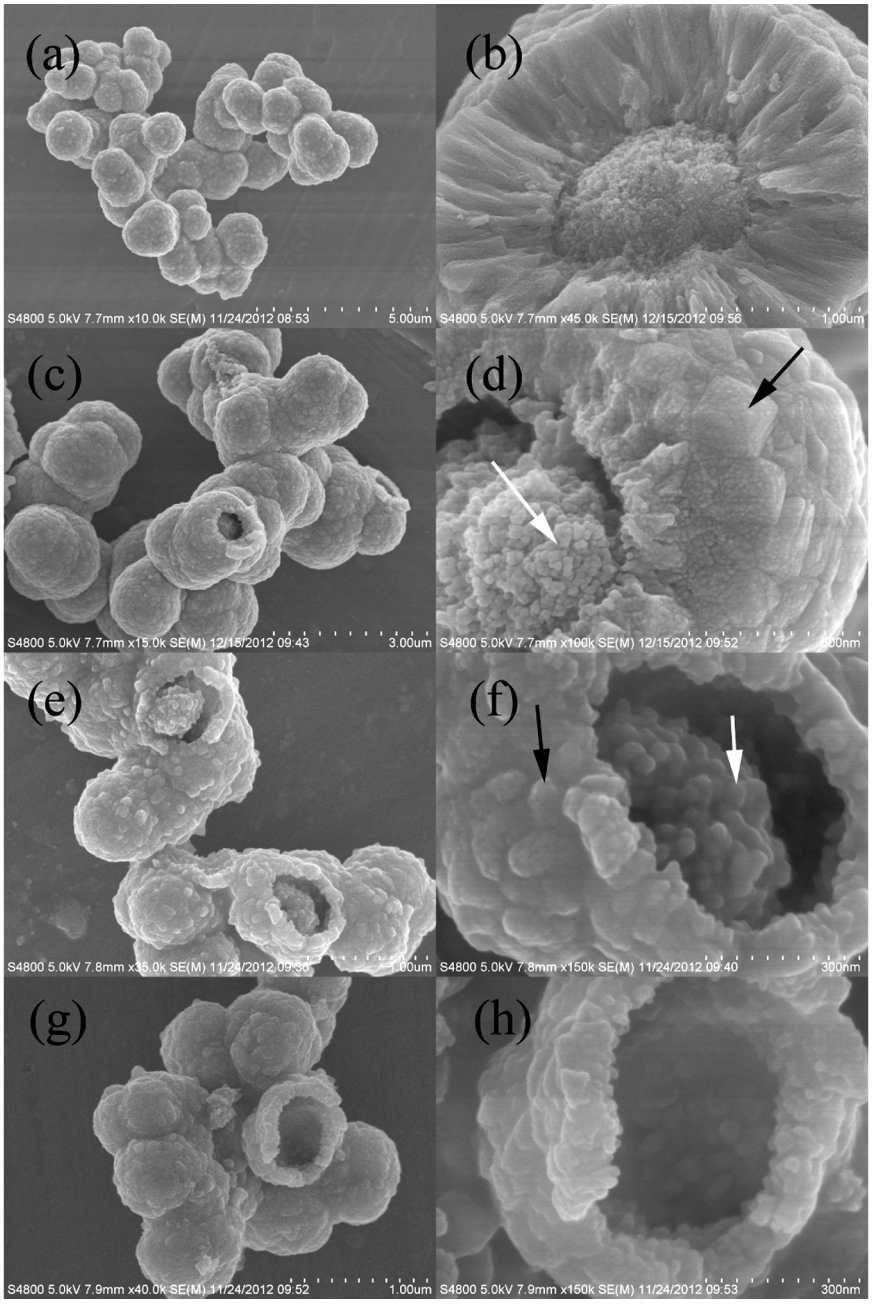

Fig. 6. SEM images of TiO_2 samples for $S_{1\text{-}3}$ (a and b), $S_{1\text{-}24}$ (c and d), $S_{15\text{-}3}$ (e and f) and $S_{15\text{-}24}$ (g and h), respectively. Black arrows indicate larger crystallites on the outer surface of the core-shell spherical structures in comparison with the smaller crystallites in the inner cores (indicated by white arrows).

3.3. *Effect of H_2O_2 on the rapid fabrication of TiO_2-HMSs*

It was found that the solution before hydrothermal reaction is deep orange, which is ascribed to the complexation between H_2O_2 and titanium ions (Eq. (4)). When compared with solvent water, H_2O_2 shows stronger affinity to Ti, which facilitates the hydrolysis of $(NH_4)_2TiF_6$ and followed by the nucleation process during the heat treatment process (Eqs. (5)–(7)). It is understandable that more nucleation centers will form in the presence of higher concentrated H_2O_2. Therefore, it is not surprising that the diameters of TiO_2 microspheres decrease with increase in the amount of H_2O_2 (Fig. 7).

The complexed H_2O_2 is unstable, which decomposes with increasing reaction time, resulting in the exposure of the surface unsaturated titanium species. These unsaturated titanium atoms are very active, which are easily dissolved into the solution in the presence of HF (Eq. (2)). According to our previous studies, HF can induce both the dissolution of the particle interior and subsequent mass transfer from the core to the external surface [39,40]. The reactions of Eqs. (1)–(3) most probably occur (FIST).

Why does the surface layer of the amorphous solid particles crystallize first? This is due to the direct contact of this surface layer with the surrounding solution. Increasing the reaction time can enhance the crystallinity of the samples (Fig. 4 and Fig. S2), and facilitates the formation of hollow interiors within solid microspheres (Fig. 6). Why do the hollow particles spontaneously form? This is because the amorphous core is not in equilibrium with the surrounding solution and has a strong tendency to dissolve due to its higher solubility and higher surface energy compared to that of the surface crystalline layer. Therefore, it is not surprising that the

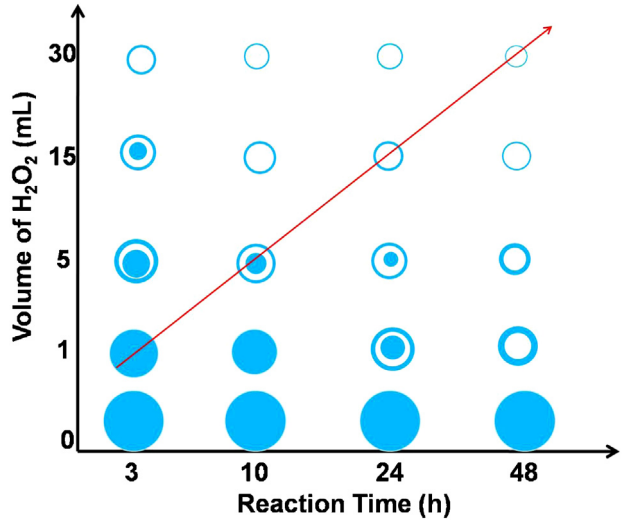

Fig. 7. Scheme illustrating the effect of H_2O_2 on the formation of TiO_2-HMSs.

interiors of the particles dissolve. This self-transformation is associated with a progressive redistribution of matter from the interior to the exterior by localized Ostwald ripening and the substantial etching caused by F [28,39].

$$(NH_4)_2TiF_6 + xH_2O_2 = 2NH_4F + Ti(O_2H)_xF_{4-x} + xHF \quad (4)$$

$$Ti(O_2H)_xF_{4-x} + (4-x)H_2O = Ti(O_2H)_x(OH)_{4-x} + (4-x)HF \quad (5)$$

$$Ti(O_2H)_x(OH)_{4-x} \rightarrow (TiO_2)_m\cdots O{-}O\cdots(TiO_2)_n \quad (6)$$

$$(TiO_2)_m\cdots O{-}O\cdots(TiO_2)_n \rightarrow TiO_2\,(\text{amorphous}) + O_2\uparrow \quad (7)$$

3.4. Adsorption and photocatalytic activity of TiO_2-HMSs

To establish the relationship between microstructures and performance of the prepared TiO_2 sample, adsorption and photocatalytic activity of the photocatalyst was evaluated using X3B, an anionic azo dye, as probe molecule, and degradation was performed under UV irradiation ($\lambda \geq 320$ nm).

Some study suggested that preliminary adsorption of substrate on the catalyst surface is a prerequisite for highly efficient oxidation [3,18,21]. In the present study, it was fond that the adsorption

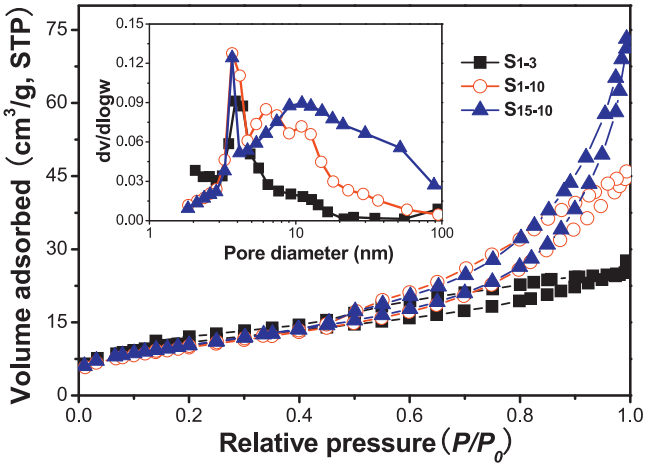

Fig. 8. Nitrogen adsorption–desorption isotherms and the corresponding pore size distributions (inset) of the TiO_2 samples.

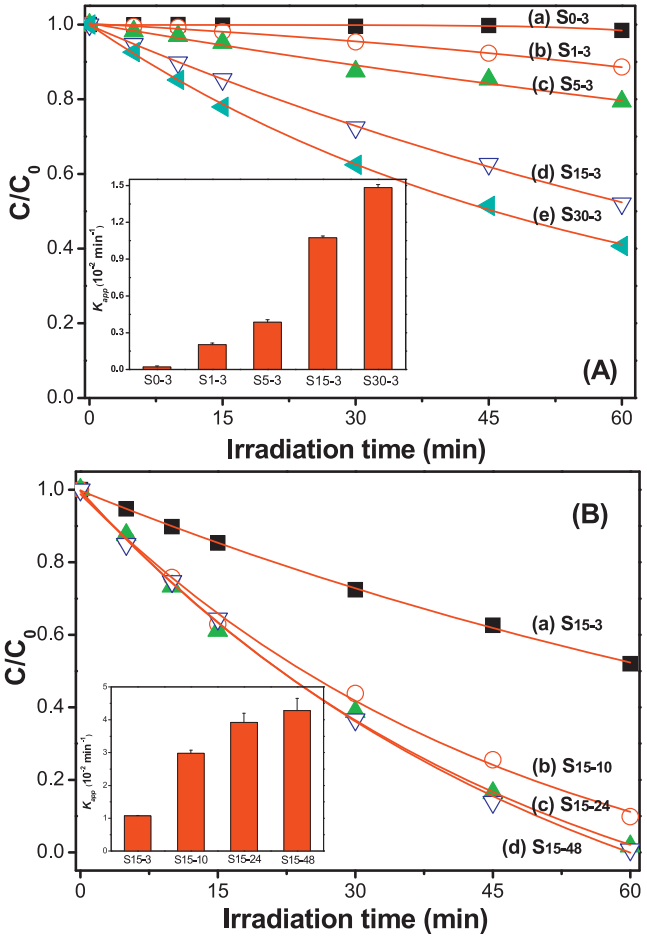

Fig. 9. Effect of H_2O_2 (A) and hydrothermal reaction time (B) on the photocatalytic activity of TiO_2 samples using X3B dye as probe under UV irradiation. Inset compares the corresponding rate constants.

of X3B dye on the surface of TiO_2-HMSs is stronger than on that of solid microspheres. With increase in the hydrothermal reaction time from 3 to 48 h, the adsorption of X3B on the surface of the TiO_2 sample prepared in the presence of 15 ml H_2O_2 steadily increases from 0.10 μmol g^{-1} to 2.18 μmol g^{-1} (Table 1). The strong adsorption of TiO_2-HMSs to X3B dye should favor for efficient electron transfer between dye and TiO_2 photocatalyst, and therefore enhance the oxidation, which will be shown below.

Fig. 9A showed the effect of H_2O_2 (0–30 ml) on the photocatalytic activity of TiO_2 samples prepared at 150 °C for 3 h. It can be seen that $S_{0\text{-}3}$ sample, which was prepared in the absence of H_2O_2, shows very low photocatalytic activity (rate consistent of only 0.022×10^{-2} min^{-1}). This is ascribed to it's poor crystallization and large diameters (Figs. 1 and 2). The photocatalytic activity of TiO_2 sample was found to steadily increase with increase in the amount of H_2O_2. The degradation rate constant soared to 1.484×10^{-2} min^{-1} in suspensions of $S_{30\text{-}3}$ sample due to H_2O_2-mediated enhanced crystallization and formation of the hollow interiors.

Fig. 9B showed the effect of hydrothermal reaction time (3–48 h) on the photocatalytic activity of TiO_2 samples prepared in the presence of 15 ml H_2O_2 at 150 °C. It can be seen that the photocatalytic activity of TiO_2 photocatalyst increases with extension the hydrothermal reaction time. The degradation rate constant of X3B in suspensions of $S_{15\text{-}3}$ is 1.074×10^{-2} min^{-1}, which is about 4 times higher than that of $S_{15\text{-}24}$ (3.922×10^{-2} min^{-1}). The enhanced photocatalytic activity can also be ascribed to the formation of TiO_2-HMSs (Fig. 6). Although the apparent degradation

rate constant of X3B on $S_{15\text{-}24}$ is smaller than on Degussa P25 TiO_2 (5.557×10^{-2} min^{-1}), a well known commercial photocatalyst (50.0 m^2 g^{-1}), both of them show similar normalized photocatalytic activity presented in unit surface area (1.012×10^{-3} $min^{-1}m^{-2}$ for $S_{15\text{-}24}$ and 1.111×10^{-3} min^{-1} m^{-2} for P25 TiO_2), also confirming the high photocatalytic activity of the prepared TiO_2-HMSs. The enhancement on the photocatalytic activity of TiO_2-HMSs is not obvious if further increase in the hydrothermal reaction time from 24 h to 48 h (Fig. 9B). This is because the hollowing process begins to stop after reaction at 150 °C for 24 h (Fig. 6).

Why do the prepared TiO_2-HMSs show superior photocatalytic activity than TiO_2 solid microspheres? This is due to the following reasons. First, good crystallization (Table 1) of TiO_2-HMSs is beneficial to reduce the number of defects, thus the recombination rates of photo-generated electrons and holes at the TiO_2-HMSs are smaller. Therefore, it is not surprising that the photocatalytic activity of TiO_2-HNP increased with increasing amount of H_2O_2 due to higher crystallinity. Second, strong adsorption favors for the degradation of the dye. As presented in Table 1, the adsorption of X3B dye on the surface of TiO_2-HMSs is stronger than on that of solid microspheres, which should favor for efficient electron transfer between dye and TiO_2 photocatalyst, and therefore enhance the oxidation.

It was reported that the photocatalytic activity of anatase TiO_2 could be greatly improved after surface fluorination [3,9]. In the present study, however, the surface-adsorbed fluoride ions have been eliminated before evaluating the photocatalytic activity by washing with 0.1 M NaOH. XPS characterization results confirmed that little fluoride ions (less than 0.3 at%) were detected on the surface of the prepared TiO_2 HMSs (Fig. S3 for $S_{15\text{-}24}$ sample as an example).

The high photocatalytic activity of TiO_2-HMSs has been attributed to multiple reflections of UV–visible light within the interior cavity that facilitates more efficient use of the light source [18]. However, UV–vis diffuse reflectance spectroscopy (DRS) characterization results showed that both solid and hollow TiO_2 microspheres have similar light-harvesting ability (Fig. S4). Therefore, it can be deduced that it is other factor than light absorption that be responsible for the high photocatalytic activity of the prepared TiO_2-HMSs.

Further experiment shows that the prepared TiO_2-HMSs can be readily separated from the slurry system by filtration or sedimentation after photocatalytic reaction and reused than the corresponding nanosized photocatalytic powders due to their large weight and good mobility. Therefore, the prepared TiO_2-HMSs are promising to be used in environmental purification.

4. Conclusions

H_2O_2 plays important role on the formation of TiO_2-HMSs, which not only improves the crystallization of priminary TiO_2 nanocrystallites, but also enhances the hollow process. A formation mechanism based on H_2O_2-assisted nucleation and followed by FIST hollowing process is put forward for the rapid fabrication of TiO_2-HMSs. The prepared TiO_2-HMSs show high photocatalytic activity due to the H_2O_2-mediated enhanced crystallization and improved adsorption to organics. The proposed route for the preparation of TiO_2-HMSs has the merits of being simple, reproducible, and easy to scale-up, which is expected to be widely used in photocatalysis, catalysis, electrochemistry, separation, purification, drug delivery and so on.

Acknowledgements

This work was supported by Program for New Century Excellent Talents in University (NCET-12-0668), National Natural Science Foundation of China (20977114 & 21373275) and Natural Science Foundation of Hubei Province (2011CDA107).

Appendix A. Supplementary data

Supplementary data associated with this article can be found, in the online version, at http://dx.doi.org/10.1016/j.apcatb.2013.10.011.

References

[1] X.B. Chen, S.H. Shen, L.J. Guo, S.S. Mao, Chem. Rev. 110 (2010) 6503.
[2] Y. Liu, L.F. Chen, J.C. Hu, J.L. Li, R. Richards, J. Phys. Chem. C 114 (2010) 1641.
[3] K.L. Lv, X.F. Li, K.J. Deng, J. Sun, X.H. Li, M. Li, Appl. Catal. B 95 (2010) 383.
[4] S.G. Kumar, L.G. Devi, J. Phys. Chem. A 115 (2011) 13211.
[5] J. Sun, X. Yan, K.L. Lv, S. Sun, K.J. Deng, D.Y. Du, J. Mol. Catal. A 367 (2013) 31.
[6] Q.J. Xiang, J.G. Yu, M. Jaroniec, Chem. Soc. Rev. 41 (2012) 782.
[7] K.L. Lv, B. Cheng, J.G. Yu, G. Liu, Phys. Chem. Chem. Phys. 14 (2012) 5349.
[8] J. Zhang, Q. Xu, Z.C. Feng, M.J. Li, C. Li, Angew. Chem. Int. Ed. 47 (2008) 1766.
[9] Z.Y. Wang, K.L. Lv, G.H. Wang, K.J. Deng, D.G. Tang, Appl. Catal. B 100 (2010) 378.
[10] X.W. Lou, L.A. Archer, Z.C. Yang, Adv. Mater. 20 (2008) 3987.
[11] H.X. Li, Z.F. Bian, J. Zhu, D.Q. Zhang, G.S. Li, Y.N. Huo, H. Li, Y.F. Lu, J. Am. Chem. Soc. 129 (2007) 8406.
[12] S.W. Liu, J.G. Yu, M. Jaroniec, J. Am. Chem. Soc. 132 (2010) 11914.
[13] Z.Y. Wang, D.Y. Luan, C.M. Li, F.B. Su, S. Madhavi, F. Boey, X.W. Lou, J. Am. Chem. Soc. 132 (2010) 16271.
[14] X.L. Wang, H.L. He, Y. Chen, J.Q. Zhao, X.Y. Zhang, Appl. Surf. Sci. 258 (2012) 5863.
[15] S.F. Xie, X.G. Han, Q. Kuang, J. Fu, L. Zhang, Z.X. Xie, L.S. Zheng, Chem. Commun. 47 (2011) 6722.
[16] L. Chen, L.F. Shen, P. Nie, X.G. Zhang, H.S. Li, Electrochim. Acta 62 (2012) 408.
[17] Y.Z. Li, T. Kunitake, S. Fujikawa, J. Phys. Chem. B 110 (2006) 13000.
[18] X.F. Li, K.L. Lv, K.J. Deng, J.F. Tang, R. Su, J. Sun, L.Q. Chen, Mater. Sci. Eng. B 158 (2009) 40.
[19] J.G. Yu, W. Liu, H.G. Yu, Cryst. Growth Des. 8 (2008) 930.
[20] X.P. Lin, D.M. Song, X.Q. Gu, Y.L. Zhao, Y.H. Qiang, Appl. Surf. Sci. 263 (2012) 816.
[21] K.L. Lv, J.G. Yu, K.J. Deng, J. Sun, Y.X. Zhao, D.Y. Du, M. Li, J. Hazard. Mater. 173 (2010) 539.
[22] S.J. Ding, J.S. Chen, Z.Y. Wang, Y.L. Cheah, S. Madhavi, X. Hu, X.W. Lou, J. Mater. Chem. 21 (2011) 1677.
[23] X.J. Cheng, M. Chen, L.M. Wu, G.X. Gu, Langmuir 22 (2006) 3858.
[24] X.X. Li, Y.J. Xiong, Z.Q. Li, Y. Xie, Inorg. Chem. 45 (2006) 3493.
[25] L. Liu, Y.M. Cui, B. Li, X.F. Zhou, W.P. Ding, Appl. Surf. Sci. 256 (2010) 2596.
[26] J.G. Yu, S.W. Liu, H.G. Yu, J. Catal. 249 (2007) 59.
[27] A.M. Collins, C. Spickermann, S. Mann, J. Mater. Chem. 13 (2003) 1112.
[28] J.G. Yu, H.T. Guo, S. Davis, S. Mann, Adv. Funct. Mater. 16 (2006) 2035.
[29] M. Liu, K.L. Lv, G.H. Wang, Z.Y. Wang, Y.X. Zhao, Y.R. Deng, Chem. Eng. Technol. 33 (2010) 1531.
[30] Z.Y. Liu, D.D. Sun, P. Guo, J.O. Leckie, Chem. Eur. J (2007) 1851.
[31] J.G. Yu, J. Zhang, Dalton Trans. 39 (2010) 5860.
[32] J. Li, H.C. Zeng, J. Am. Chem. Soc. 129 (2007) 15839.
[33] J.H. Pan, X.W. Zhang, A.J. Du, D.D. Sun, J.O. Leckie, J. Am. Chem. Soc. 130 (2008) 11256.
[34] J.G. Yu, L. Shi, J. Mol. Catal. A 326 (2010) 8.
[35] S.W. Liu, J.G. Yu, S. Mann, Nanotechnology 20 (2009) 325606.
[36] S.W. Liu, J.G. Yu, B. Cheng, M. Jaroniec, Adv. Colloid Interf. Sci. 173 (2012) 35.
[37] H.G. Yang, H.C. Zeng, J. Phys. Chem. B 108 (2004) 3492.
[38] Q.D. Truong, T.S. Lec, H.T. Hoa, CrystEngComm 14 (2012) 4274.
[39] K.L. Lv, J.G. Yu, J.J. Fan, M. Jaroniec, CrystEngComm 14 (2011) 7044.
[40] J.H. Cai, Z.Y. Wang, K.L. Lv, Y. Zheng, J.G. Yu, M. Li, RSC Adv. 3 (2013) 15273.
[41] K.L. Lv, Y.M. Xu, J. Phys. Chem. B 110 (2006) 6204.
[42] K.L. Lv, J.C. Hu, X.H. Li, M. Li, J. Mol. Catal. A 356 (2012) 78.
[43] Y.K. Du, J. Rabani, J. Phys. Chem. B 110 (2006) 6123.